This document was prepared for the ETI by third parties under contract to the ETI. The ETI is making these documents and data available to the public to inform the debate on low carbon energy innovation and deployment.

Programme Area: Marine

Project: PerAWAT

Title: Development of a Computational Fluid Dynamics Model for a Horizontal Axis Tidal Current Turbine

Abstract:

This deliverable is concerned with the computational fluid dynamics modelling of an unducted horizontal-axis tidal current turbine, with the aim to construct and verify a numerical model that can be used as a tool to investigate and parameterize the wake behind a tidal current turbine. The work is described in two main sections: first the preliminary work to better understand the turbine using more basic modelling approaches, and then the development and application of the CFD model of the turbine. This deliverable forms the foundation to all other deliverables in this work package.

Context:

The Performance Assessment of Wave and Tidal Array Systems (PerAWaT) project, launched in October 2009 with £8m of ETI investment. The project delivered validated, commercial software tools capable of significantly reducing the levels of uncertainty associated with predicting the energy yield of major wave and tidal stream energy arrays. It also produced information that will help reduce commercial risk of future large scale wave and tidal array developments.

PerAWaT MA1003

Development of a computational fluid dynamics model for

a horizontal axis tidal current turbine

WG3 WP5 D1

Participant lead and report author: Dr Gareth I Gretton
Work package leader and report checker: Prof David M Ingram

The University of Edinburgh

Version: 1.0
29th October 2010

Executive summary

This report documents the work done for and represents deliverable one of WG3 WP5 (device scale numerical modelling: detailed CFD of other concepts). This work may be grouped into three areas of activity: one, interrogating the geometry; two, sub-component grid verification; and three, determination of the non-rotor turbine geometry. The first of these – interrogation of the geometry – has shown that the generic turbine is unlikely to operate as originally predicted due to the thickness of the blade section and the highly turbulent environment in which the blade will operate. It has also shown that there are some subtleties to consider in the generation of the geometry for the CFD model. The second activity has provided important grid verification information for the construction of the full CFD model, and has led to the resolution of problems encountered with the generation of grids in Ansys ICEM and their import into Code_Saturne. Finally, the third area of activity has defined a suitable ancillary geometry based on engineering considerations.

Contents

1 Introduction and context

Deliverable one of WG3 WP5 (device scale numerical modelling: detailed CFD of other concepts) is concerned with the computational fluid dynamics modelling of an un-ducted horizontal-axis tidal current turbine. The starting point for this is the turbine rotor geometry provided to the project by TGL (Thake, 2010), and a significant proportion of the work done for this project has been on properly interrogating this geometry; the understanding of which is critical to future deliverables of this work package. Also completed is grid verification of turbine sub-components and the generation of the complete turbine geometry.

Within the context of the presently discussed work package, this deliverable forms a foundation to the work on all subsequent deliverables. For D2, whilst the geometry and meshing approach for the rotor itself will be different, the mesh in the far-field will be similar. The model setup in the solver will also share a number of similarities. For D3 (parametric description of wakes) and D4 (effects of turbulence and device interaction) a well-constructed model is of course fundamental.

With regards to the wider project, the most significant linkages are with WG3 WP1 (device scale numerical modelling: single device performance and wake) and WG3 WP4 (device and array scale tool development). For the former work package the present deliverable is a dependency of the third deliverable; although in practice the two work packages involve interaction on a weekly basis; something which is proceeding successfully as will be seen from the frequent references in this report to collaborative work. For WG3 WG4 the dependence is from the fourth and final deliverable of the present work package.

2 Interrogating the rotor geometry

2.1 Preliminary remarks

The generic turbine rotor geometry was provided to the project by TGL in two forms: first, a spreadsheet giving the twist, chord, thickness ratio and section profile as a function of radius (table 1); and second, a CAD (IGES) file of this geometry. The blade section profile chosen is a NACA 6-series section having variable thickness ratio from 18% at the tip to 55% towards the root (hub-wards of which the section becomes circular). The designation is thus 63_x-$4yy$

(a=1.0), where the subscript '*x*' denotes the (variable) extent of the low-drag range and the '*yy*' indicates the variable thickness ratio. Details of this section, and an explanation of the meaning of the other numbers in the designation, are provided in (Abbott and von Doenhoff, 1959).

This rotor was designed by using published formulae for the optimum chord and twist as a function of overall and local radius, the number of blades, the design tip speed ratio and the lift coefficient at the maximum lift to drag ratio. The thickness ratio at a given radius was then arrived at according to structural considerations. As section data for NACA 6-series sections are only available in the literature for thickness ratios up to 21%, the data for the 63_3-418 section were used to obtain the lift coefficient at maximum L/D for all radial stations in the above design process. Similarly, when this turbine geometry was analysed by GH using the Tidal Bladed blade element momentum analysis tool, the 18% thick section data was again used for all sections.

Given the uncertainty over how the rotor would perform with the thicker sections, it was felt essential to first investigate the performance of these thicker sections using CFD. Although

Table 1: *Blade geometry*

Radius (m)	Twist (deg)	Chord (m)	Thickness ratio	Profile
1.25	32.5	1.612	1.000	Circle
2.05	23.2	2.271	0.550	$63_{(318)}$-455
2.45	19.9	2.119	0.533	$63_{(318)}$-453
2.85	17.2	1.962	0.511	$63_{(318)}$-451
3.25	14.9	1.813	0.485	$63_{(318)}$-449
3.65	13.1	1.677	0.454	$63_{(318)}$-445
4.05	11.5	1.556	0.422	$63_{(318)}$-442
4.45	10.2	1.447	0.390	$63_{(318)}$-439
4.85	9.1	1.351	0.359	$63_{(318)}$-436
5.25	8.1	1.265	0.330	$63_{(318)}$-433
5.65	7.2	1.189	0.306	$63_{(318)}$-431
6.05	6.4	1.120	0.286	$63_{(318)}$-429
6.45	5.8	1.058	0.275	$63_{(318)}$-427
6.85	5.2	1.003	0.267	$63_{(318)}$-427
7.25	4.6	0.953	0.255	$63_{(318)}$-426
7.65	4.2	0.907	0.243	$63_{(318)}$-424
8.05	3.7	0.865	0.227	$63_{(318)}$-423
8.45	3.3	0.827	0.208	$63_{(318)}$-421
8.85	3.0	0.792	0.188	$63_{(318)}$-419
9	2.8	0.600	0.180	63_3-418

not originally intended as part of the work programme, this has a number of benefits. First, it forms part of a more detailed sub-component verification and validation exercise; and second, the section data thus generated can be used in the blade element momentum model to arrive at a more accurate model of the turbine, thus allowing the 'full-turbine' CFD simulations to be better targeted.

Clearly the blade section coordinates are required to set up these models, as they were required to generate the CAD model provided by TGL. This highlighted the fact that there are a number of ways to generate the section geometry, as there is no analytical definition for the NACA 6-series profiles. In particular, three methods were identified:

1. Use of an inverse design program, such as that written by Ladson et al. (1996). This might be termed the 'true' method.

2. Scaling of an existing thickness distribution, as published by Abbott and von Doenhoff (1959), before addition of the camber line.

3. Scaling of an existing cambered section, with the coordinates again coming from Abbott and von Doenhoff (1959).

The lattermost method was used by TGL, but this will have the effect of shifting the lift curve as the camber will also be scaled. The significance of this was again unknown, but again it was felt necessary to investigate by means of a CFD study.

A final aspect of the blade geometry which might be noted here is the treatment of the trailing edge. The NACA 6-series sections are designed to have a sharp trailing edge, whereas in practice a blunt trailing edge is often used for practical reasons, and as specified in the TGL CAD file. This appears to be 1% of the thickness along the entire blade. The significance of this was also briefly investigated.

2.2 CFD setup

The CFD setup for the present work on 2D blade sections has been strongly informed by previous work by the present authors, e.g. Gretton (2009). This previous work was completed using the commercial software Ansys CFX as opposed to Code_Saturne, but choices such as the turbulence model (SST-k-ω) and grid design (see figure 2), remained as previous, thus providing a
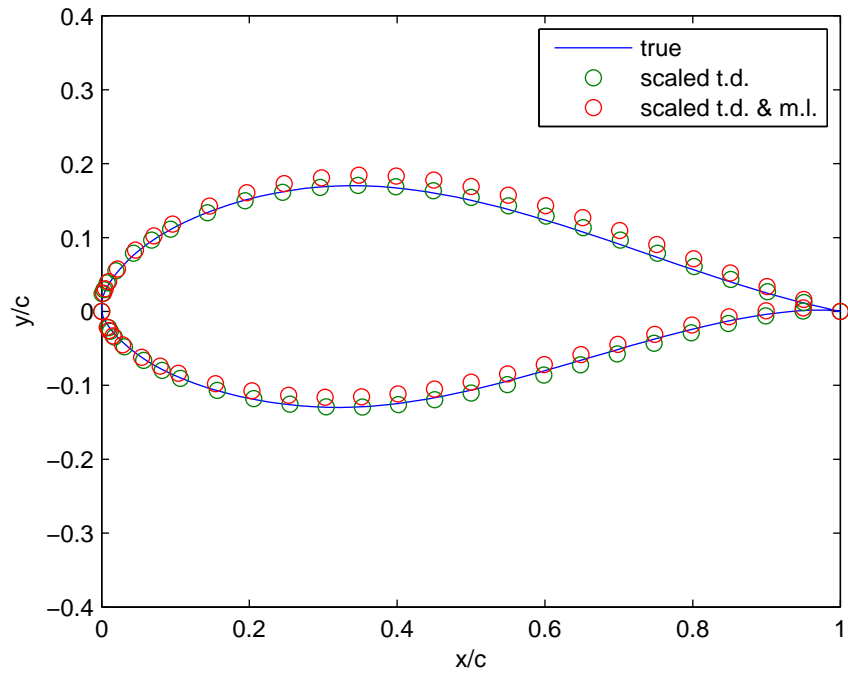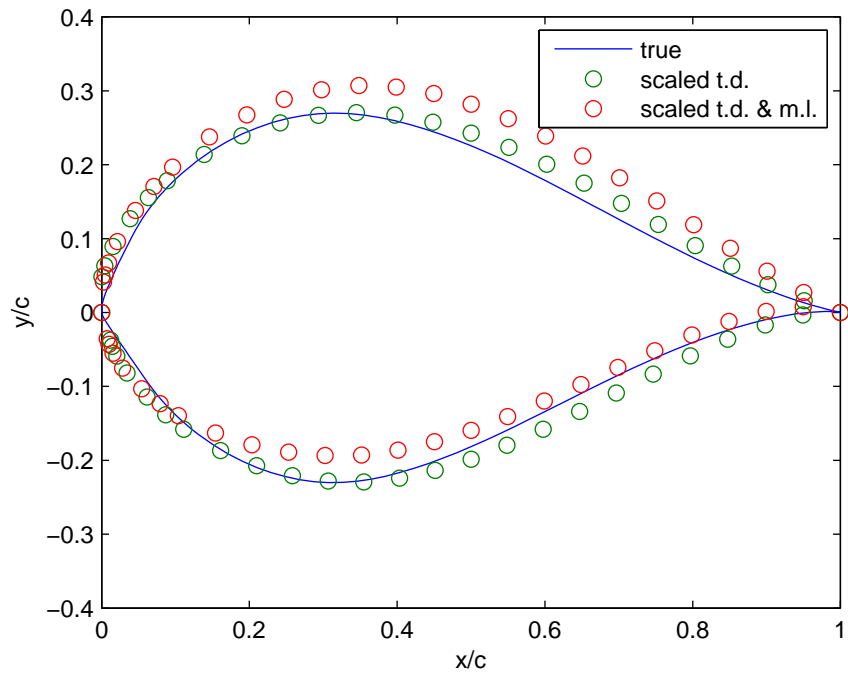
Figure 1: *Plots of the 63_x-430 and 63_x-450 sections (top and bottom), as derived using three methods: inverse design method (labelled 'true'); scaling of the thickness distribution before adding the camber; and a scaling of a cambered section*

significant level of confidence in the current work. The boundary conditions specified were as follows: on the inlet the velocity, turbulence kinetic energy (k) and turbulence eddy dissipation rate (ε) were fixed; on the outlet the pressure was fixed; on the foil surfaces a no-slip condition was imposed; and on the 'front' and 'back' faces of the 1-volume thick 3D mesh, symmetry conditions were imposed to force a 2D flow.

All of these boundary conditions could be imposed directly through the graphical user interface of Code_Saturne with the exception of the turbulence parameters on the inlet. These were thus specified through a Fortran user subroutine. Values for k and ε were selected to produce a turbulence intensity of 0.1% and a length scale of 0.1 m at the foil, by allowing for the decay from the inlet. The inlet velocity, and the constant values of the density and viscosity in the domain, were chosen to produce a Reynolds number of 3×10^6.

Grid convergence studies for these 2D blade section simulations are discussed later in section 3.1.

2.3   2D blade section results – variable thickness

Section data for a range of thicknesses are shown in figure 3; the coordinates in all cases were obtained from the inverse design program of Ladson et al. (1996). The trends for both the lift and drag coefficients are clear and need little explanation: as the thickness ratio increases the lift-curve slope decreases, the maximum lift decreases and the drag coefficient increases; thus the thicker sections unambiguously behave less well. Simulations of a 50% thick profile were also attempted but there was insufficient time to adequately quality assure the results and so they are not included here.

2.4   2D blade sections results – alternative coordinate definitions

The significance of different ways of generating a 63_x-430 section profile is shown in figure 4. It is clear that the profiles generated by the inverse design method and by scaling of the thickness distribution prior to adding camber behave similarly, whereas the more strongly cambered profile, generated by scaling an already cambered profile, shows a significant shift in the lift curve.

(a)

(b)
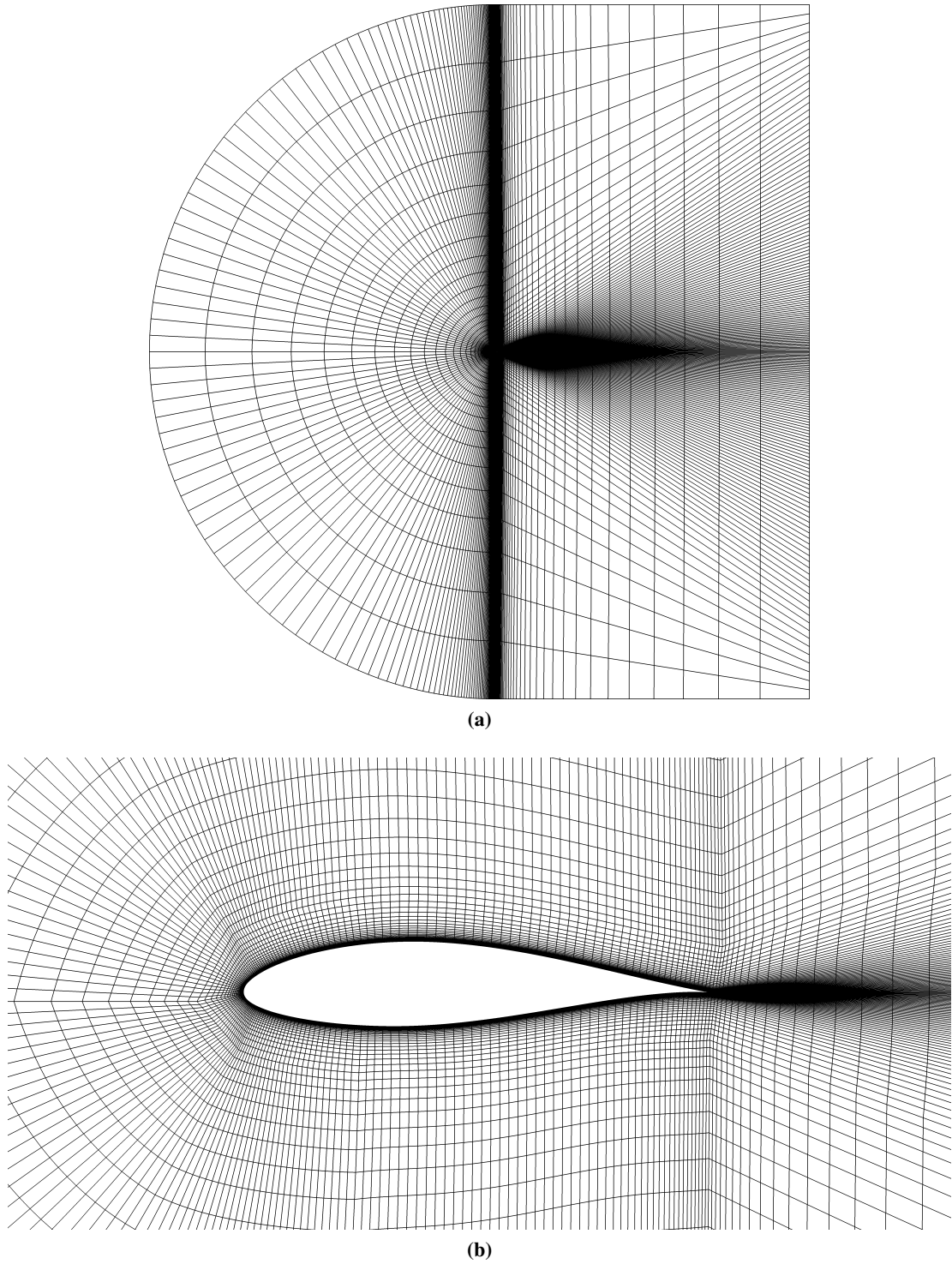
Figure 2: *Views of the grid for the* $63_3 - 418$ *geometry as per Ladson. The top view (a) shows the complete grid while the bottom view (b) shows the grid in the vicinity of the foil.*

Figure 3: *Coefficients of lift and drag versus angle of attack for various profile thickness rations. All profile coordinates were determined using the inverse design method of Ladson et al. (1996).*

Figure 4: *Coefficients of lift and drag versus angle of attack for a 63ₓ-430 section, with coordinates derived using three methods (c.f. figure 1).*

12

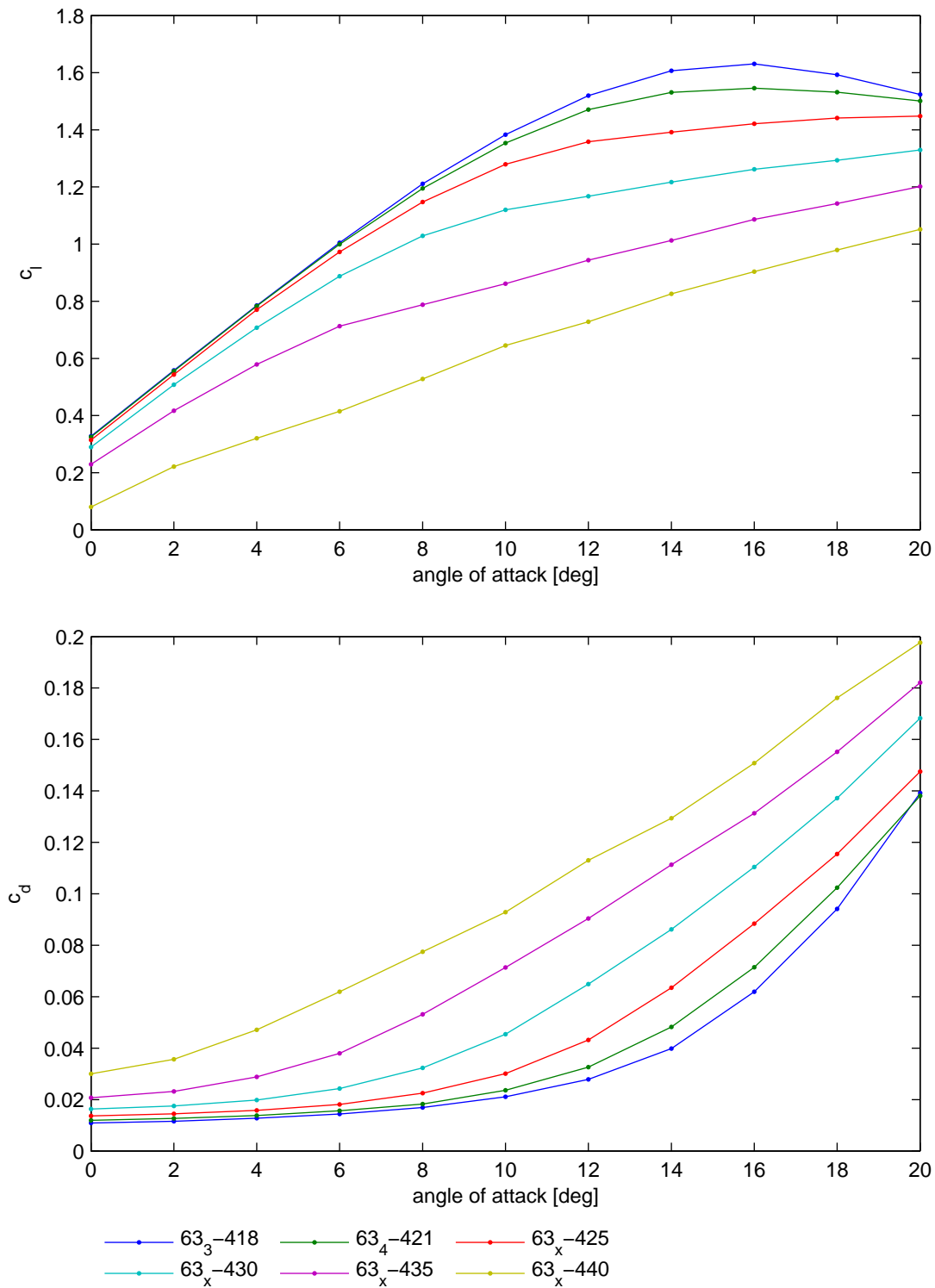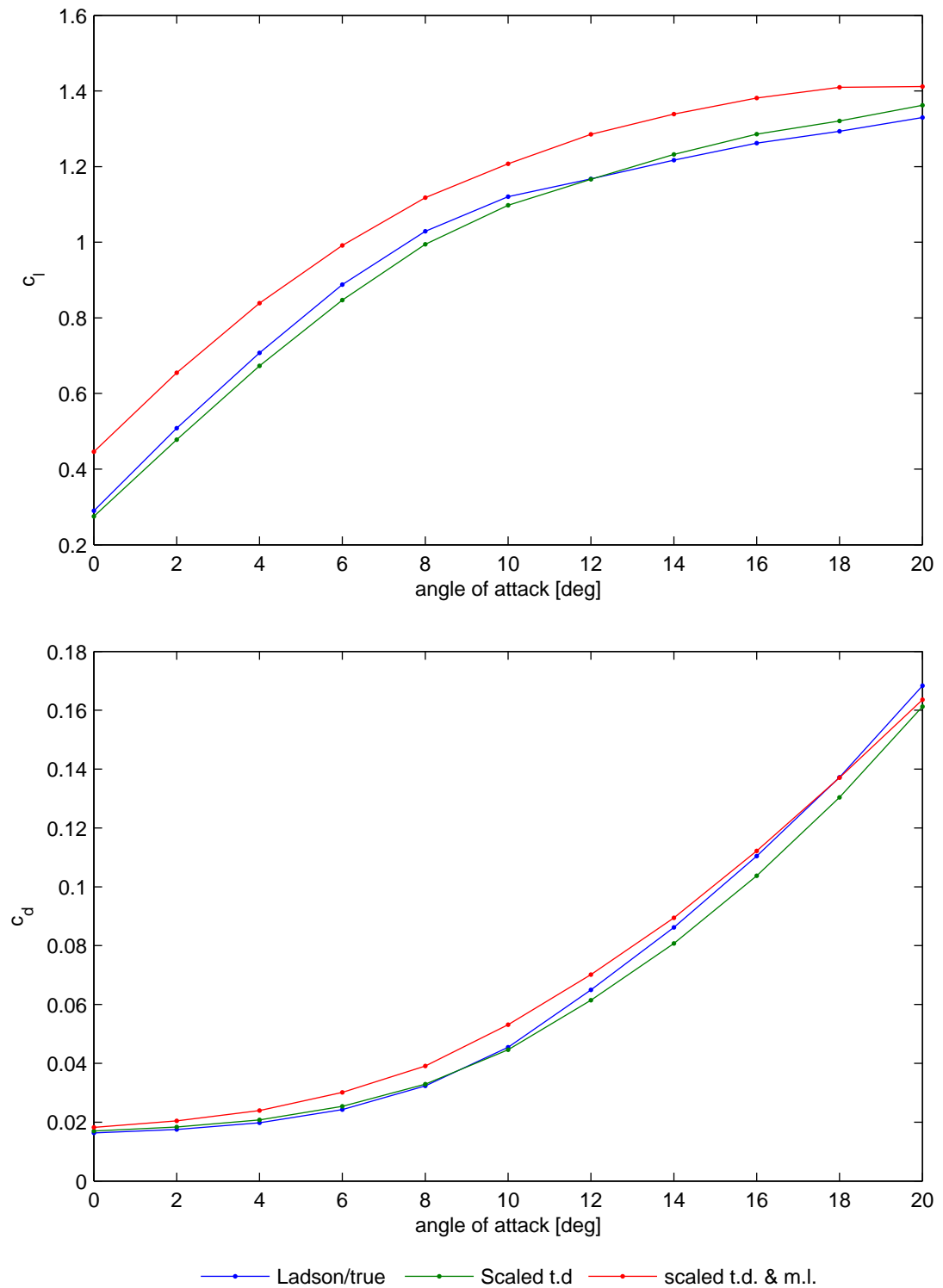## 2.5   2D blade sections results – sharp and blunt trailing edges

Figure 5 shows how the choice of a sharp or blunt trailing edge, and the choice in grid spacing towards the trailing edge for the blunt case, affects the section characteristics. In the first blunt trailing edge case the streamwise spacing remains the same as in the sharp trailing edge case, whereas in the second the spacing at the trailing edge is reduced by an order of magnitude while the number of nodes in the streamwise direction remains the same. It is clear from the results that for small angles of attack the difference between all three cases is minimal, whereas for larger angles of attack it is seen that it is necessary for the grid spacing to be decreased at the trailing edge in order to properly capture the flow features created by the blunt trailing edge (i.e., a blunt trailing edge solution with insufficient grid spacing at the trailing edge behaves as a sharp trailing edge solution). These flow physics differences are elucidated in figure 6 where it is shown how the blunt trailing edge case with reduced streamwise spacing predicts the presence of a counter-rotating (relative to the main trailing edge recirculation zone) vortex at the trailing edge.

The relevance of the above is as follows: it is common practice in CFD studies to 'artificially' sharpen what is in practice (i.e. physically) a blunt trailing edge in order to reduce computational requirements. As has been demonstrated above, for moderate angles of attack, as will be incident on the turbine blade, the difference in performance (between sharp and blunt trailing edges) is minimal. Based on this analysis, therefore, it would be considered desirable to proceed with a sharp trailing edge geometry for the turbine model. Unfortunately, and as will be discussed in section 3.2, there are further factors to consider when moving to a 3D grid.
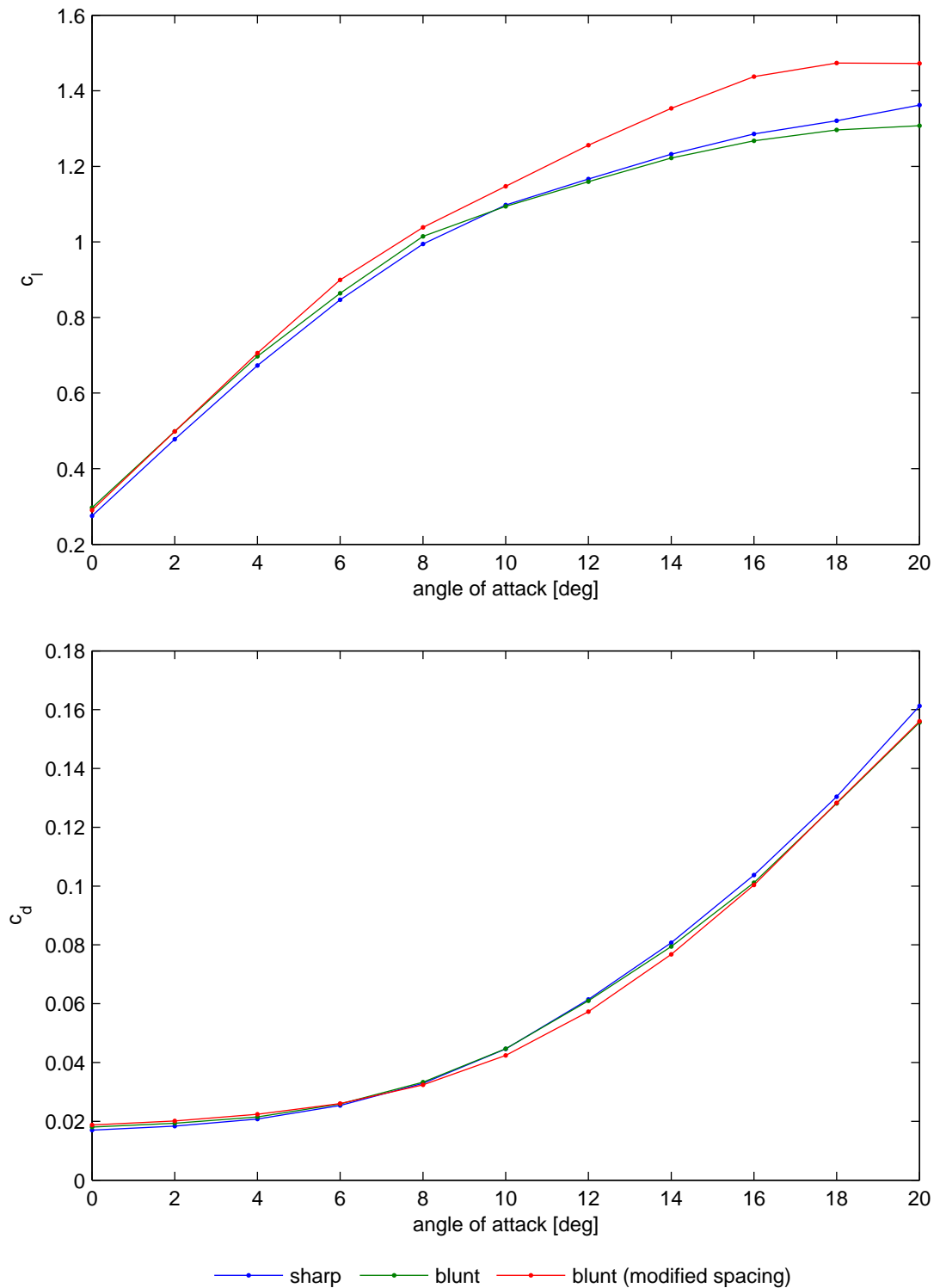
Figure 5: *Coefficients of lift and drag versus angle of attack for sharp and blunt trailing edges for a 63$_x$-430 section. In the case of the blunt trailing edge there are results from two grids, the first having the same streamwise spacing as the sharp trailing edge grid, and the second having decreased spacing towards the trailing edge ('modified spacing').*

(a)

(b)

(c)

Figure 6: *Contour and vector plots of the velocity field towards the trailing edge of a 63ₓ-430 section at an angle of attack of 8°. As with figure 5 there are two results for the blunt trailing edge case: standard (b) and modified (c) spacings.*

2.6   2D blade sections results – validation

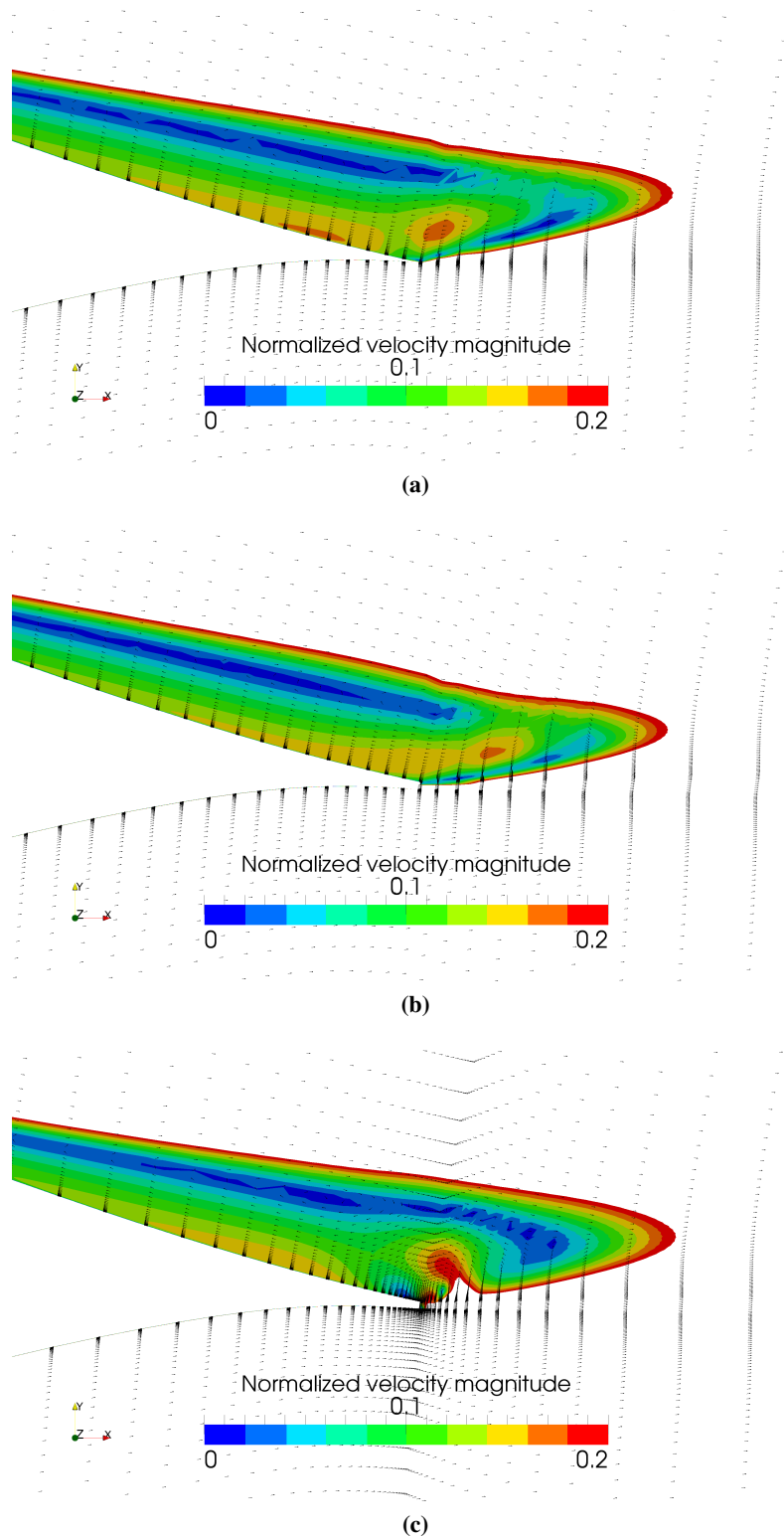Validation of the present CFD results for the 63_3-418 and 63_4-421 sections is given in figures 7 and 8. As indicated, the present CFD results are for a Reynolds number of 3×10^6, while Abbott and von Doenhoff provide data for Reynolds numbers of 3×10^6 and 6×10^6 in the case of natural transition and a Reynolds number of 6×10^6 for tripped flow. Being fully turbulent simulations, the tripped data offer the most relevant comparison to the present CFD, subject to the caveat that the data from Abbott and von Doenhoff are perhaps 'over-tripped' in the sense that the trip strip is unnecessarily rough. This over-tripping is perhaps responsible for the reduced lift values in the experimental data. Overall, and for angles of attack below stall, it is felt that the comparison is good, for both profiles.

Figure 7: *Coefficients of lift and drag versus angle of attack for the 63_3-418 – comparison of present CFD results (geometry from inverse design method) with data from Abbott and von Doenhoff (1959).*
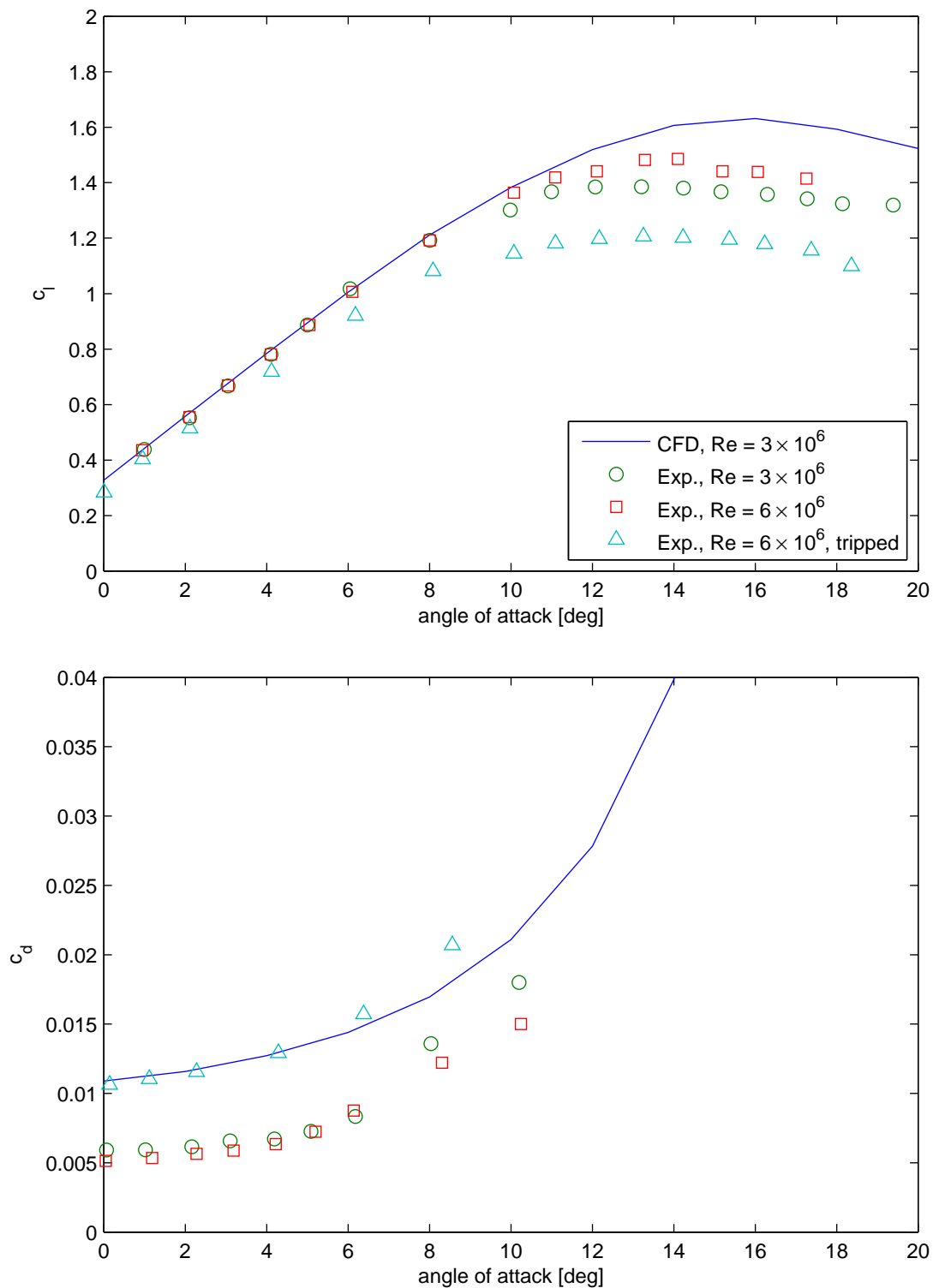
Figure 8: *Coefficients of lift and drag versus angle of attack for the 63₄-421 – comparison of present CFD results (geometry from inverse design method) with data from Abbott and von Doenhoff (1959).*
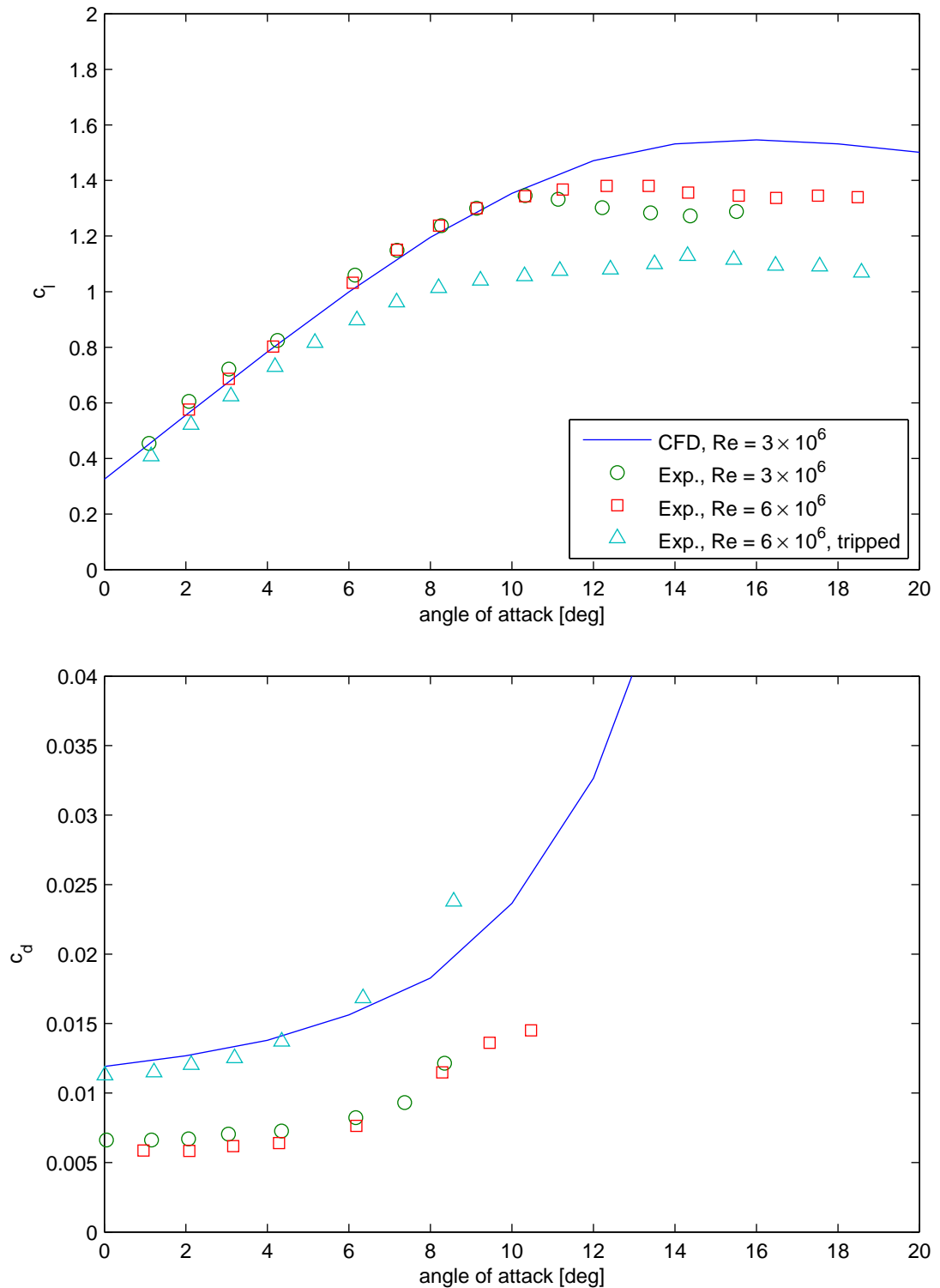
2.7 GH Tidal Bladed results

As discussed above, the section data of figure 3 may be used to improve the Tidal Bladed model of the turbine (Whelan, 2010). For blade stations where the section thickness is less than or equal to 40% the data is interpolated from that shown in figure 3 whereas for thicknesses larger than this the data for the 40% thick section is simply used. The results, along with those from the 'original' model which used the experimental data for the 63_3-418 section, are shown in figure 9. Clearly the difference is significant. Further, the differences would be even more significant if section data for thicknesses up to 50% were considered.

Also shown in this figure are results from Oxford (**?**), produced using an in-house BEM code and with section data from Xfoil (Drela and Youngren, 2001) with tripped boundary layers. (Note that this in-house code has been validated by comparison with Tidal Bladed.) Two predictions are made: the first uses Xfoil data for variable thickness sections which have been scaled from a cambered 63_3-418 section (as discussed above), while the second uses Xfoil data for variable thickness sections produced using the Ladson program. Both of these predictions use section data for thicknesses up to 50%. Again there are significant differences between these two predictions, which shows the importance of the means by which the section coordinates are generated. It might also be noted here that additional results from Oxford (**?**) have shown that the significant turbine performance degradation relative to the original predictions using 18% thick section data and with natural transition are due to the change to variable thickness section data and to tripped data; neither change alone accounting for the difference in the results.

Overall, it might be concluded that there is significant uncertainty in the turbine performance, but that the present exercise has reduced this uncertainty. The Bladed Predictions using the present CFD data believed to be the most accurate, based on the quality and relevance of the section data, with the omission of data for sections thicker than 40% being likely to be offset by the 3D effects near the root of the blade.

2.8 Interim conclusions

This section of the report has explored a number of key issues related to the turbine rotor geometry:
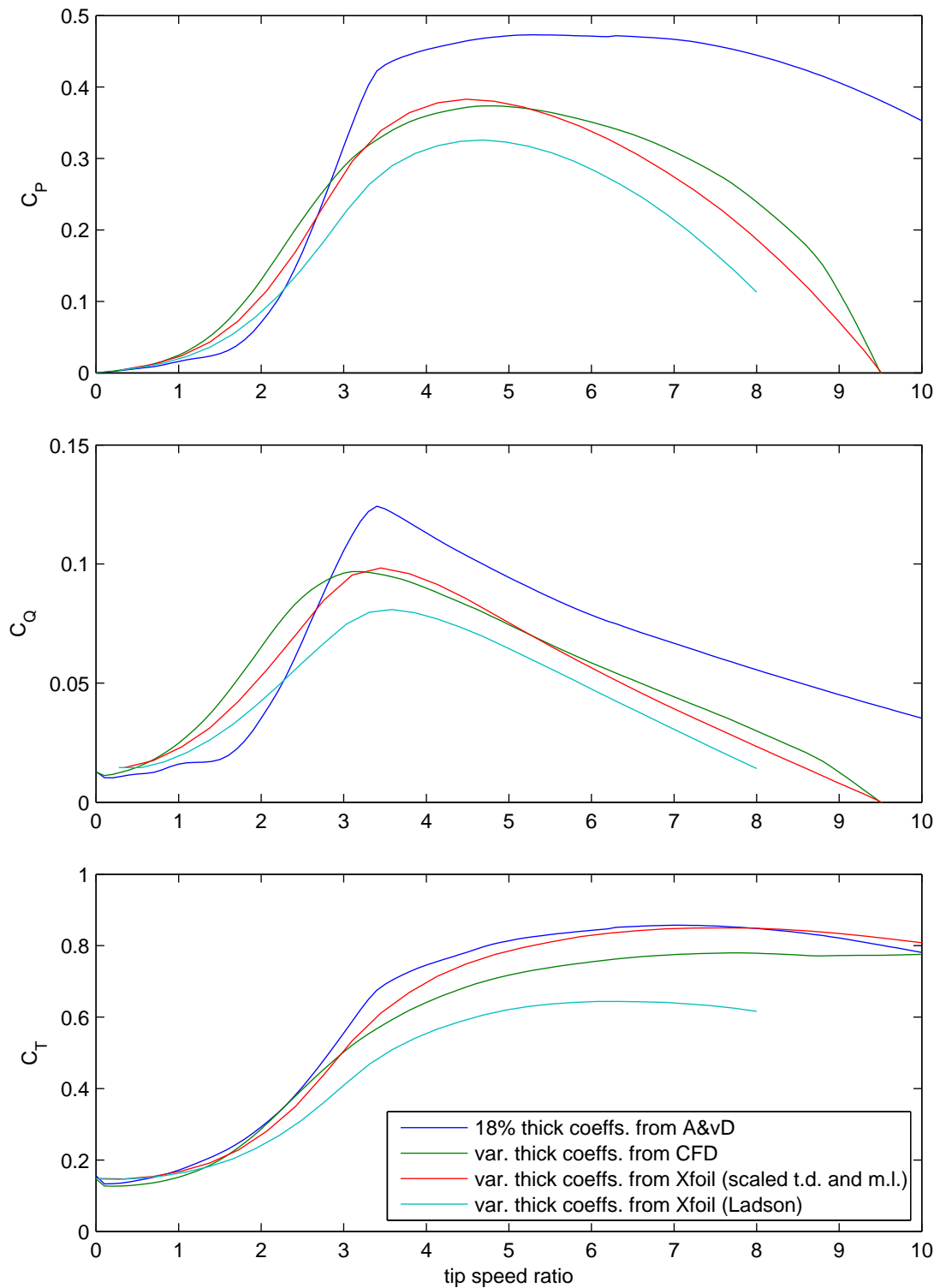
Figure 9: *Coefficients of power, torque and thrust for the turbine, as predicted from Tidal Bladed, using section data for the 63_3-418 from Abbott and von Doenhoff (1959) and using section data as per figure 3, and as predicted using an in-house BEM code at Oxford with Xfoil data.*

1. section 2.3 has shown the significant variation in section behaviour according to the thickness to chord ratio.

2. section 2.4 has shown the importance of the precise section form, and that the scaling of an already cambered section, as was done to produce the geometry in the IGES file supplied to the project, results in a significant shift in the lift-curve.

3. section 2.5 has shown that for moderate angles of attack there is comparatively little difference between sharp and blunt trailing edge geometries. It has also shown that for higher angles of attack, where differences become apparent, the trailing edge region must be well resolved.

The significance of the fist two of these issues has then been demonstrated by recourse to blade element momentum models of the turbine.

3   Sub-component grid verification

3.1   2D blade sections

As noted in section 2.2, the CFD setup for the current work on 2D blade sections, including the selection of the grid, is informed by previous work. This previous work focused on thinner blade sections than are typical of the present rotor geometry and so it was decided to carry out a grid verification exercise on the $63_x - 430$ section. This exercise used three grids, termed 'coarse', 'medium' and 'fine'. The medium grid has 268 cells in the wrap-around direction (with 196 on the foil surface) and 82 cells in the wall-normal direction. The coarse and fine grids contain respectively half and double the number of cells in these two directions, thus giving one quarter and four times the number of cells in the mesh.

This study was carried out for angles of attack between zero and twenty degrees in two degree increments, with the results for the convergence of the lift and drag coefficients being given in tables 2 and 3. All of the parameters given are as standard in the literature on grid convergence (e.g. Roache, 1998; NPARC, 2008). The conclusions that may be draw are as follows. For the lift coefficient there is good convergence for moderate angles of attack (up to about 8-10°) and less good thereafter, with errors on the medium grid (as used for all of the simulations in the previous section) being low ($< 6\%$) for angles of attack up to 8°, rising notably thereafter. For

the drag coefficient, the convergence is more problematic, with a number of cases showing oscillatory convergence ($-1 < R < 0$). Further, for the angles of attack which do show monotonic convergence, and where grid convergence indices can be calculated, there is no clear pattern, such as was observed for the lift coefficients. Given these inconclusive results, we therefore refer to past experience (Gretton, 2009) which suggests that errors in the drag coefficient are likely to be higher than those for the lift coefficient. With regards to the accuracy of the turbine simulations, this is of less importance because turbine performance is more strongly driven by the lift coefficient.

Table 2: *Grid convergence study for the 63_x-430: Lift values.*

	c_l						GCI		
α	coarse	medium	fine	$h = 0$	R	p	m-c	f-m	ratio
0	0.321	0.290	0.282	0.279	0.25	2.00	4.59	1.18	0.97
2	0.548	0.508	0.498	0.495	0.24	2.03	3.18	0.79	0.98
4	0.761	0.707	0.696	0.693	0.21	2.25	2.53	0.54	0.98
6	0.956	0.888	0.868	0.859	0.30	1.75	4.05	1.24	0.98
8	1.122	1.029	0.997	0.981	0.34	1.55	5.85	2.06	0.97
10	1.249	1.120	1.059	1.003	0.48	1.07	13.11	6.63	0.95
12	1.343	1.167	1.055	0.849	0.65	0.63	34.10	24.37	0.90
14	1.435	1.217	1.089	0.907	0.59	0.77	31.86	20.92	0.89
16	1.508	1.262	1.129	0.970	0.54	0.88	28.90	17.54	0.89
18	1.536	1.293	1.168	1.033	0.52	0.95	25.18	14.45	0.90
20	1.528	1.330	1.193	0.885	0.69	0.53	41.80	32.25	0.90

Table 3: *Grid convergence study for the 63_x-430: Drag values.*

	c_d						GCI		
α	coarse	medium	fine	$h = 0$	R	p	m-c	f-m	ratio
0	0.0169	0.0163	0.0159	0.0131	0.86	0.21	25.07	22.23	0.97
2	0.0178	0.0175	0.0170		2.05				
4	0.0193	0.0198	0.0193		−0.97				
6	0.0223	0.0242	0.0239		−0.19				
8	0.0279	0.0323	0.0324	0.0325	0.03	5.01	0.55	0.02	1.00
10	0.0367	0.0454	0.0466	0.0468	0.14	2.85	3.88	0.52	1.03
12	0.0476	0.0649	0.0678	0.0684	0.17	2.57	6.76	1.09	1.04
14	0.0622	0.0862	0.0884	0.0887	0.09	3.41	3.59	0.33	1.03
16	0.0816	0.1104	0.1118	0.1119	0.05	4.38	1.65	0.08	1.01
18	0.1042	0.1372	0.1349		−0.07				
20	0.1337	0.1683	0.1587		−0.28				

3.2   3D blade tip

The simulation of wing tip flows serves as a useful sub-component to analyse, given the similarity with the flow at the turbine blade tip. The case chosen was that of (Chow et al., 1997) which had been simulated numerically by (Dacles-Mariani et al., 1995) and more recently by (Craft et al., 2005, 2006). These references provide some guidance on the grid resolution required, but unfortunately do not provide a complete picture of the grid topology adopted. A useful discussion of this issue (gridding of wing tips) was found in (Spentzos et al., 2005; Spentzos, 2005).

Three different strategies were attempted in the current work, as shown in figures 10, 11 and 12. The first attempt, a C-O-grid with a collapsed trailing edge block, proved unsuccessful due to problems with the Code_Saturne import of the CGNS file format. In particular this was due to inconsistent definitions of cells and faces having collapsed edges, as occur with collapsed blocks. Preliminary fixes for this problem have subsequently been introduced into Code_Saturne, but full resolution of the issue will not occur until a subsequent release.

The second attempt, an extruded C-grid with a Y-grid blocking on the tip proved successful where the latter had failed (by avoiding collapsed blocks), but unfortunately introduced an overly complicated block topology in the meshing program (Ansys ICEM). This related to the definition of O-grid indices: where the C-O grid had only a single O-grid index, thus allowing simple navigation through the grid, the Y-grid blocking introduced four O-grid indices. It was thus felt that in practice, and especially in the context of a full turbine mesh, this strategy was simply not workable.

The third attempt, a C-H-O-grid, forces the use of a blunt trailing edge (which it was preferred to avoid, in order to reduce computational cost, as discussed in section 2.5), but leads to a comparatively simple block topology as with the C-O-grid, whilst avoiding the collapsed block. Thus, given the importance of developing a practicable blocking strategy for the complete turbine, this option has been adopted.

3.3   2D tower simulations

The spacings required in the streamwise and wall normal directions on the tower were determined by recourse to the literature on circular cylinder flows e.g. (Celic and Shaffer, 1995;

(a)

(b)

(c)
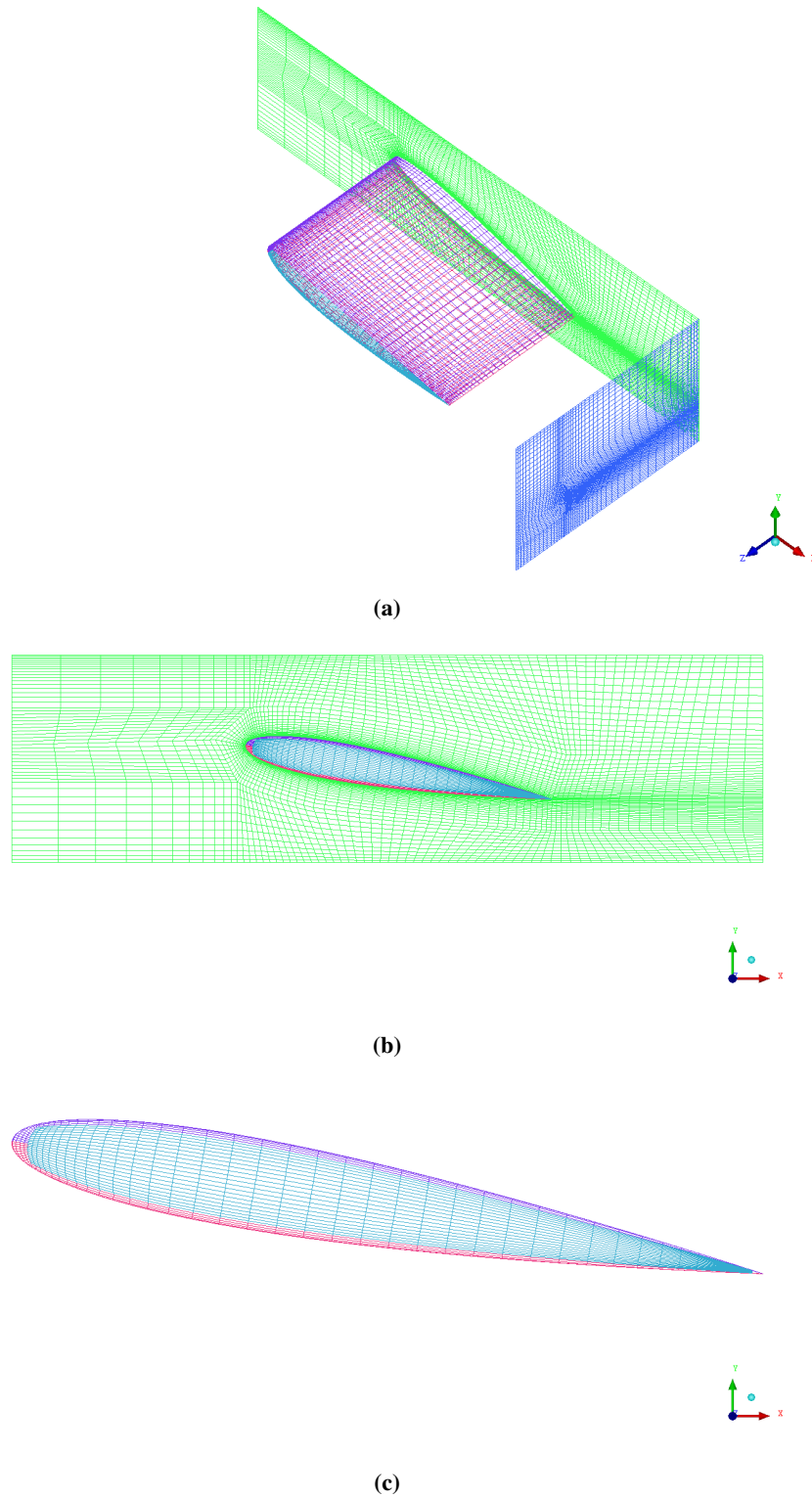
Figure 10: *Three views of the C-O-grid with collapsed trailing edge block.*

(a)

(b)

(c)
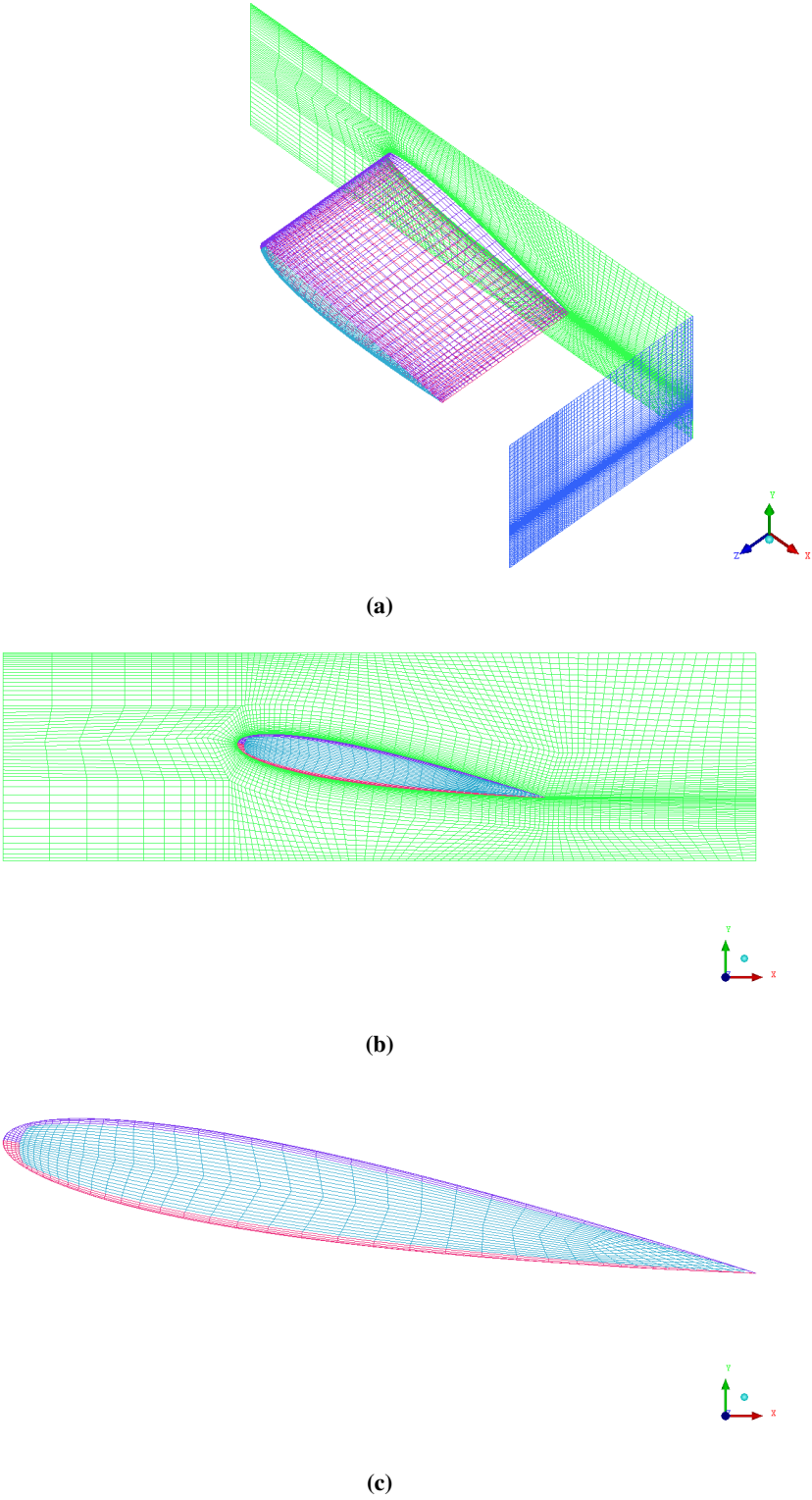
Figure 11: *Three views of the extruded C-grid with Y-grid on the tip.*
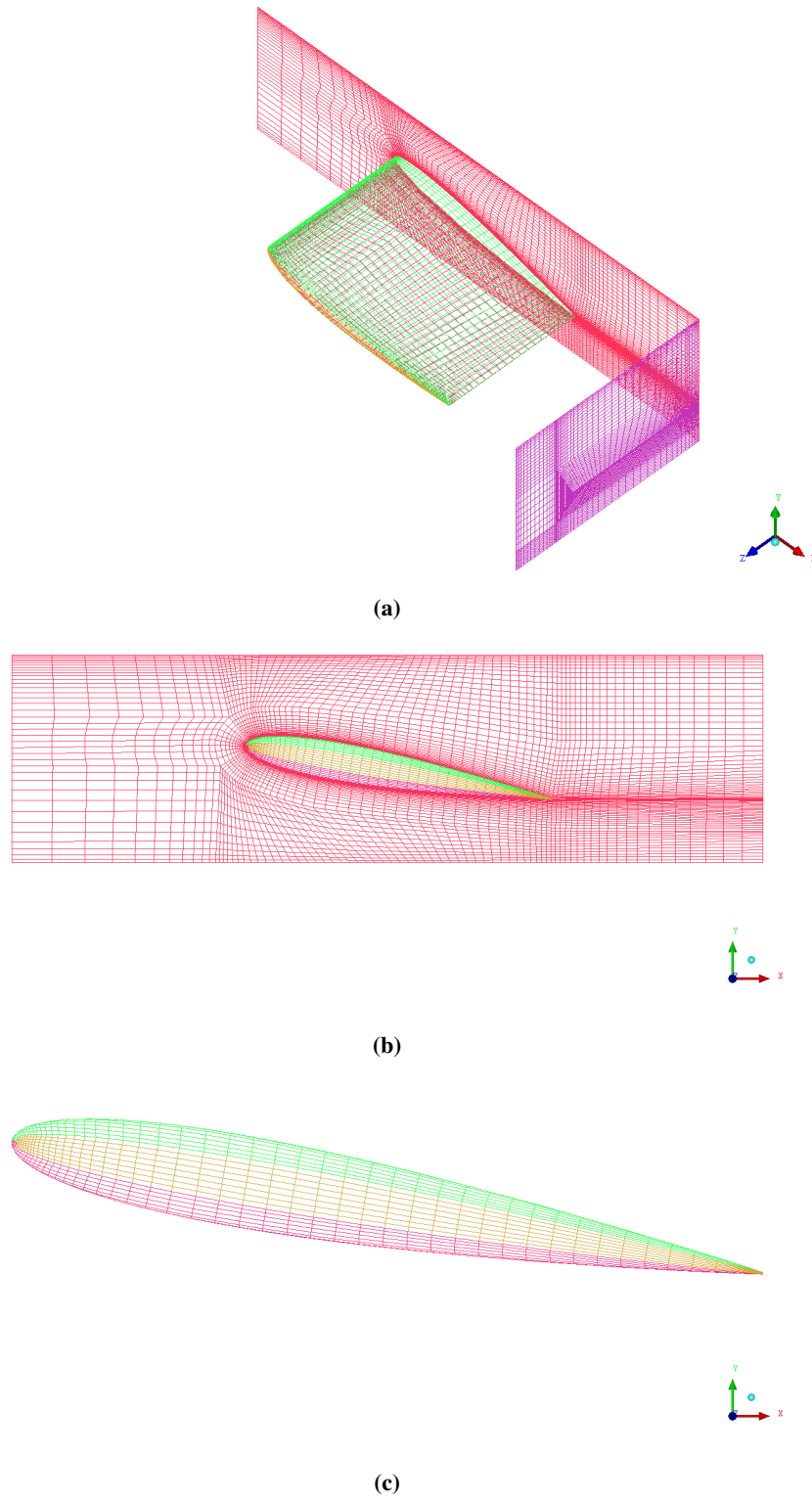
(a)

(b)

(c)

Figure 12: *Three views of the C-H-O-grid.*

Richmond-Bryant, 2003). In general, the node requirements are found to be comparable to those for blade sections.

4 Turbine (non-rotor) geometry

As discussed previously, the design of the rotor was provided by TGL, whereas no details were provided for what might be termed the 'ancillary geometry'; namely the design of the hub, nacelle and tower. A suitable design for these components was determined by a variety of engineering considerations by the team at the University of Oxford, with input from the present authors. All parameters are noted in table 4 and are discussed below. A 3D view is shown in figure 13.

Regarding the nacelle, the volume of this was taken to be equal to the volume of a 1 MW Vestas wind turbine, this being 41 m^3. The basic premise here is that the volume of the components contained in the nacelle – primarily the gearbox, generator and transformer – will be related most strongly to the rated power, and so will be equivalent for a 1 MW tidal current turbine. A number of arguments may be made for why the volume of a tidal current turbine nacelle would be greater or smaller; for example, given the lower rotational speeds of the blades, either a larger gearbox or a larger generator would be required; whereas against this, the increased potential for cooling might suggest a smaller nacelle. Given the difficulty of assessing these considerations, the volume was simply taken to be equivalent. The ratio of diameter to length was set by visual consideration of existing designs, and a cylindrical form was chosen to allow rotating frame of reference CFD simulations to be conducted. A 0.5 m fillet was added at the rear of the nacelle to potentially reduce the nacelle wake.

The hub diameter was taken as being the same as the nacelle, this being a good match to the end of the blade as provided by TGL. The hub length was taken to be 2 m (somewhat larger than the 1.6 m chord length of the blade at the root). Extending upstream of the hub, an elliptical nose cone (ratio 1:1.5) was added, having its major axis in the streamwise direction.

Finally, the tower diameter was chosen by conducting a basic stress analysis. This considered the tower as a monopile, with the turbine acting as a point load 18 m from the sea bed. The thrust load for the turbine was determined by assuming a thrust coefficient of one and a free stream speed of 3 m/s. A load factor of 1.35 was applied to this, based on the guidance for

offshore wind turbine structures in DNV (2007). A yield stress for mild steel of 240 MPa was taken, along with a material factor of 1.10, again from DNV (2007). Finally, based on a wall thickness of 50 mm, a diameter of 2 m is required.

Table 4: *Turbine geometry*

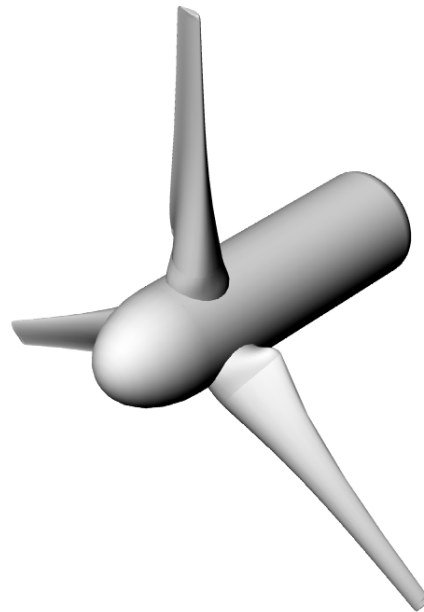| Parameter	Value
Rotor diameter	18 m
Nacelle diameter	3 m
Nacelle length	5.8 m
Nacelle fillet radius	0.5 m
Hub length	2 m
Nose-cone length	2.25 m
Nose-cone shape	Ellipse, 1:1.5
Tower diameter	2 m

Figure 13: *3D view of the turbine geometry (excluding tower)*

5   Acceptance criteria

The acceptance criteria for the present deliverable are as follows:

1. Model will include:

    (a) Geometry of the moving rotor and any hydrodynamically active surfaces

    (b) Model designed for prototype scale (as defined in WG0) in a typical water depth (defined in WG0) with no waves.

    (c) Grid converged quality assured models generated (the point at which your results are no longer statistically varying)

2. Report will include:

    (a) Description of model methodology including all algorithms and assumptions

    (b) Wake described with sufficient detail to allow a parameterization to be made.

    (c) Assessment of model performance via comparison with data from WG3 WP1

    (d) Discussion of sensitivities and limitations.

With regards to the model composition (1), the geometry is described in sections 2 and 4 for prototype scale, with a typical water depth being chosen as twice the diameter (36 m). Grid convergence is determined by sub-component grid verification as discussed in section 3.

Report acceptance criteria (a) and (d) are contained heretofore. (b) is implicit, with the parameterization itself being deliverable three of the present work package. Some comparison of data from WG3 WP1 (as per d) has already been achieved, but more will be possible when the relevant deliverables of that work package are subsequently delivered.

References

Abbott, I. H. and von Doenhoff, A. E. (1959), *Theory of Wing Sections*, Dover.

Celic, I. and Shaffer, F. D. (1995), Long time-averaged solutions of turbulent flow past a circular cylinder, *International Journal for Numerical Methods in Fluids*, 56, pp. 185–212.

Not to be disclosed other than in line with the terms of the Technology Contract

Chow, J., Zilliac, G., and Bradshaw, P. (1997), Turbulence measurements in the near field of a wing tip vortex, Technical Memorandum 110418, NASA.

Craft, T. J., Launder, B. E., and Robinson, C. M. E. (2005), The computational modelling of wing-tip vortices and their near-field decay, in W. Rodi and M. Mulas (eds.), *Engineering Turbulence Modelling and Measurement 6*, Elsevier, Amsterdam.

Craft, T. J., V., G. A., Launder, B. E., and Robinson, C. M. E. (2006), A computational study of the near-field generation and decay of wingtip vortices, *International Journal of Heat and Fluid Flow*, 27, pp. 684–695.

Dacles-Mariani, J., Zilliac, G., Chow, J., and Bradshaw, P. (1995), Numerical/experimental study of a wingtip vortex in the near field, *AIAA Journal*, 33, pp. 1561–1568.

DNV (2007), Design of offshore wind turbine structures, Offshore Standard DNV-OS-J101.

Drela, M. and Youngren, H. (2001), *Xfoil 6.9 User Primer*.
    URL http://web.mit.edu/drela/Public/web/xfoil/

Gretton, G. I. (2009), *The hydrodynamic analysis of a vertical axis tidal current turbine*, Ph.D. thesis, School of Engineering, University of Edinburgh.

Ladson, C. L., Brooks, C. W. J., Hill, A. S., and Sproles, D. W. (1996), Computer program to obtain ordinates for NACA airfoils, Technical Memorandum 4741, NASA.

NPARC (2008), *Examining spatial (grid) convergence*, [Accessed 4th February 2009].
    URL http://www.grc.nasa.gov/WWW/wind/valid/tutorial/spatconv.html

Richmond-Bryant, J. (2003), Verification testing in computational fluid dynamics: an example using Reynolds-averaged Navier-Stokes methods for two-dimensional flow in the near wake of a circular cylinder, *International Journal for Numerical Methods in Fluids*, 43, pp. 1371–1389.

Roache, P. J. (1998), *Verification and Validation in Computational Science and Engineering*, Hermosa, Albuquerque, New Mexico, USA.

Spentzos, A. (2005), *CFD Analysis of 3D Dynamic Stall*, Ph.D. thesis, Aerospace Engineering, University of Glasgow.

Spentzos, A., Barakos, G., Badcock, K., Richards, B., Wernert, P., Schreck, S., and Raffel, M. (2005), Investigation of three-dimensional dynamic stall using computational fluid dynamics, *AIAA Journal*, 43(5), pp. 1023–1033.

Thake, J. (2010), Email correspondence from TGL to EDF and GH on 21st January 2010.

Whelan, J. I. (2010), GH rotor design – WG4 WP1 D1, Document number 104330/BT/02, dated 25th February.